Compact stationary fluxons in the Josephson junction ladder

Andrii O. Prykhodko

Kyiv Academic University, 36 Vernadsky blvd., Kyiv 03142, Ukraine and Bogolyubov Institute for Theoretical Physics, National Academy of Sciences of Ukraine, vul. Metrologichna 14B, 03143 Kyiv, Ukraine

Ivan O. Starodub and Yaroslav Zolotaryuk*

Bogolyubov Institute for Theoretical Physics, National Academy of
Sciences of Ukraine, vul. Metrologichna 14B, 03143 Kyiv, Ukraine
(Dated: November 25, 2025)

Stationary compact fluxon profiles are shown to be exact solutions of the inductively coupled and dc-biased Josephson junction ladder. Such states do not exist in the parallel Josephson junction array which is described by the standard discrete sine-Gordon equation. It is shown that there are compact fluxon and multi-fluxon states which either satisfy the top-bottom antisymmetry or are asymmetric. The anti-symmetric states have zero energy if their topological charge is even and the asymmetric states always have zero energy. Depending on the anisotropy constant the compact fluxons can either coexist with the non-compact states or only compact states are possible. External magnetic field prevents compact state existence.

I. INTRODUCTION

Josephson junction ladders (JJLs) have attracted a significant interest from researches because of their nontrivial statistical [1, 2] and dynamical properties [3]. There are several non-trivial wave phenomena that exist in JJLs and are not possible in the standard parallel arrays which a described by the discrete sine-Gordon (or Frenkel-Kontorova) model [4]. Discrete breathers or intrinsic localized modes were discovered experimentally [5, 6] and this discovery opened a new chapter in the studies of the Josephson junction based systems. There is a flat band in the JJL plasmon spectrum [7, 8], and, again, no such a thing is possible in the parallel array. Starting from the pioneering work [9] a significant number of results have been obtained concerning the stationary vortex (or fluxon) properties in JJLs under the influence of the external magnetic field. Stationary fluxon properties in JJL were investigated in [10]. Trias and coworkers [11] performed detailed studies of the fluxon-discrete breather interactions.

In this work we demonstrate that an important family of stationary fluxon states in JJLs was overlooked. Since an JJL has a flat band in its linear spectrum, it is logical to expect it to have, alongside with the exponentially decaying fluxons, completely compact fluxons. Under the term "compact" we understand the exact steplike solutions which has the phase distribution of the type $0, \dots, 0, 2\pi, 2\pi, \dots, 2\pi$. We will demonstrate the existence of these solutions, compare them to the noncompact fluxons and compute the energy of the both. It will be shown that their existence depends strongly on the JJL anisotropy.

The importance of this work can be viewed from an-

other angle. Researchers working in the area of nonlinear lattice dynamics study discrete compactons [12, 13], solutions that are localized on several particles while the rest of the lattice is at equilibrium. The solutions we are discussing in this paper are not dynamical, they are static. However, they have topological charge. To our knowledge, this is the first report about compact topological excitations in the realistic physical system.

II. MODEL AND EQUATIONS OF MOTION

In this work the 2-row ladder of small Josephson junctions is studied. The elementary cell of the Josephson junction ladder consists of three junctions, as shown in Fig. 1. Dynamics of each of these junctions is described by the Josephson phase which is the difference of the superconducting wavefunction phases. The Josephson phases that belong to the nth elementary cell will be denoted as follows: the vertical phase $\phi_n^{(v)}$, the bottom horizontal $\phi_{n,1}^{(h)}$ and the top horizontal $\phi_{n,2}^{(h)}$ phases. In total the ladder consists of N+1 vertical junctions, N top horizontal and N bottom horizontal junctions. Each vertical junction is biased by the external dc current, I_B .

The Hamiltonian function of the whole JJL is based on the resistively and capacitively shunted model and can be

^{*}Electronic address: yzolo@bitp.kyiv.ua

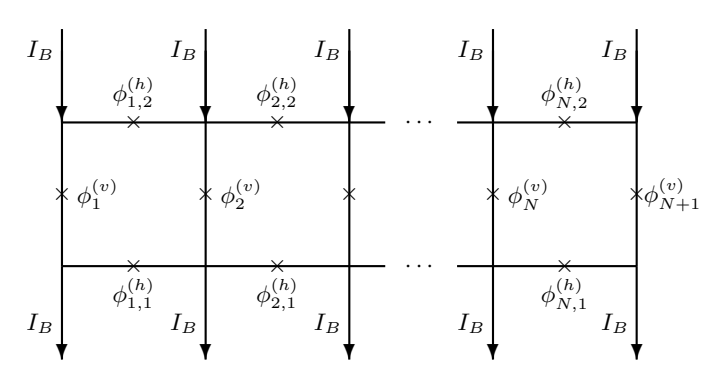


FIG. 1: Schematic view of the dc-biased 2-row ladder with open ends. Crosses correspond to the Josephson junctions.

written as follows:

$$H = E_K + U_J + U_L, \tag{1}$$

$$E_K = \frac{C_v}{2} \sum_{n=1}^{N+1} \left(\frac{\hbar \dot{\phi}_n^{(v)}}{2e} \right)^2 + \frac{C_h}{2} \sum_{n=1}^{N} \sum_{k=1}^2 \left(\frac{\hbar \dot{\phi}_{n,k}^{(h)}}{2e} \right)^2, \quad (2)$$

$$U_J = \sum_{n=1}^{N+1} \left[E_J^{(v)} (1 - \cos \phi_n^{(v)}) - I_B \phi_n^{(v)} \right] +$$

$$+\sum_{n=1}^{N}\sum_{k=1}^{2}E_{J}^{(h)}(1-\cos\phi_{n,k}^{(h)}),\tag{3}$$

$$U_L = \frac{\Phi_0^2}{8\pi^2 L} \sum_{n=1}^{N} \left(\phi_{n+1}^{(v)} - \phi_n^{(v)} + \phi_{n,2}^{(h)} - \phi_{n,1}^{(h)} - 2\pi f \right)^2 . (4)$$

Here $E_J^{(v,h)} = \hbar I_c^{(v,h)}/(2e)$ is the Josephson coupling energy for the vertical (superscript $^{(v)}$) or horizontal (superscript $^{(h)}$) junctions. The critical currents and capacitances of the junctions are given by $I^{(v,h)}$ and $C_{v,h}$, respectively. The frustration parameter $f = \Phi_e/\Phi_0$ is the ratio of the external magnetic field flux to the flux quantum $\Phi_0 = \pi \hbar/e$. As one can see, the total energy is divided into three parts: the total energy all of the capacitors, E_K , the total Josephson energy, U_J , and the inductive energy, stored in all JJL cells (loops), U_L . The JJL can be interpreted as a 6N+2-dimensional hamiltonian system with E_K being its kinetic energy and U_J+U_L being its potential energy.

The equations of motion for the Josephson phases of the ladder can either be deduced from the above Hamiltonian or can be obtained from the Kirhoff equations, Josephson equations for each of the juncions and the flux quantization realtion for each loop. Since these equations of motion have been derived in the number of previous papers [6, 11] we will not repeat the derivation procedure here. We introduce the dimensionless time $t \to t\omega_p$, where $\omega_p = \sqrt{2\pi I_c^{(v)}/(\Phi_0 C_v)}$ is the Josephson plasma frequency. We also introduce the following dimensionless

parameters:

$$\frac{1}{\beta_L} = \frac{\Phi_0}{2\pi L I_c^{(v)}}, \ \gamma = \frac{I_B}{I_c^{(v)}}, \ \eta = \frac{I_c^{(h)}}{I_c^{(v)}} = \frac{C_h}{C_v} = \frac{R_v}{R_h},$$

$$\alpha = \frac{\hbar \omega_p}{2eR_v I^{(v)}}, \tag{5}$$

where $R_{v,h}$ is the vertical (horizontal) junction resistance, β_L^{-1} describes the JJL discreteness, γ is dimensionless external current, η is the anisotropy constant and α is the dissipation parameter associated the normal electron tunneling. The anisotropy constant describes whether the energy is concentrated mostly in the vertical subsystem ($\eta \ll 1$) or in the horizontal one ($\eta \gg 1$). Finally, one ends up with the dimensionless set of evolution equations which are, in fact, a system of coupled discrete sine-Gordon (DSG) equations. For the sake of brevity we introduce

$$\mathcal{N}(x) \equiv \ddot{x} + \alpha \dot{x} + \sin x. \tag{6}$$

The final equations have the following form:

$$\mathcal{N}(\phi_n^{(v)}) = \gamma + \frac{1}{\beta_L} \left(\hat{\mathfrak{D}} \phi_n^{(v)} + \right) \tag{7}$$

$$+\phi_{n,2}^{(h)} - \phi_{n,1}^{(h)} - \phi_{n-1,2}^{(h)} + \phi_{n-1,1}^{(h)}$$
, $n = \overline{1, N+1}$,

$$\mathcal{N}(\phi_{n,k}^{(h)}) = -(-1)^k \frac{\Delta_{n+1,n}}{\eta \beta_L}, \ k = 1, 2, \tag{8}$$

$$\Delta_{n+1,n} \equiv \phi_{n+1}^{(v)} - \phi_n^{(v)} + \phi_{n,2}^{(h)} - \phi_{n,1}^{(h)} - 2\pi f, \tag{9}$$

together with the boundary conditions:

$$\mathcal{N}(\phi_1^{(v)}) = \gamma + \frac{1}{\beta_L} \Delta_{2,1},\tag{10}$$

$$\mathcal{N}(\phi_{N+1}^{(v)}) = \gamma - \frac{1}{\beta_L} \Delta_{N+1,N},\tag{11}$$

where $n=\overline{1,N}$ stands for $n=1,2,\ldots,N$. The discrete laplacian operator in Eq. (7) is defined as $\hat{\mathfrak{D}}\phi_n\equiv\phi_{n+1}-2\phi_n+\phi_{n-1}$. A careful look at Eq. (8) reveals that the dynamical equations for the top and bottom junctions reproduce each other when the top-bottom inversion transform $\phi_{n,1}^{(h)}\to-\phi_{n,2}^{(h)}$ is applied. However, we are not going to exclude one of the horizontal components with the help of this antisymmetry and will solve the full system of equations.

The dimensionless JJL energy is obtained by introducing the parameters (5) and normalizing the energy (1)-(4) to the Josephson energy of the vertical junction $(E_J^{(v)})$:

$$H = \sum_{n=1}^{N} \frac{1}{2} \left[\dot{\phi}_{n}^{(v)2} + \eta \sum_{k=1}^{2} \dot{\phi}_{n,k}^{(h)2} \right] + \frac{1}{2} \dot{\phi}_{N+1}^{(v)2} +$$

$$+ \frac{1}{2\beta_{L}} \sum_{n=1}^{N+1} \left(\phi_{n+1}^{(v)} - \phi_{n}^{(v)} + \phi_{n,2}^{(h)} - \phi_{n,1}^{(h)} - 2\pi f \right)^{2} +$$

$$+ \sum_{n=1}^{N+1} \left[1 - \cos \phi_{n}^{(v)} - \gamma \phi_{n}^{(v)} \right] + \eta \sum_{n=1}^{N} \sum_{k=1}^{2} (1 - \cos \phi_{n,k}^{(h)}).$$
(12)

From this formula one can clearly understand the physical meaning of the anisotropy constant η . It characterizes the ratio of the energy stored in the subsystem of horizontal junctions to the energy of the vertical subsystem.

III. PROPERTIES OF COMPACT AND NON-COMPACT FLUXONS

In this section the properties of the compact states as well as their differences with respect to the non-compact fluxons.

A. Compact fluxons

Fluxons are topological excitaions that connect two different ground states of the JJL. They carry the integer number of the magnetic flux quanta and are characterized by the topological charge, $Q \in \mathbb{Z}$. For example, the fluxon with Q=1 connects the minima with $\phi_n^{(v)}=\arcsin\gamma$ and $\phi_n^{(v)}=2\pi+\arcsin\gamma$. Careful analysis of the r.h.s. of Eqs. (7)-(11) shows that compact solutions can be exist as fixed points of the system if no magnetic field is applied (f=0). Consider the stationary case $\dot{\phi}_n^{(v)}=0$ $(n=\overline{1,N+1})$, $\dot{\phi}_{n,k}^{(h)}=0$ $(n=\overline{1,N1},k=1,2)$. If all the vertical phases correspond to the solutions of the equation $\sin\phi_n^{(v)}=\gamma$ and the horizontal phases satisfy $\sin\phi_{n,m}^{(h)}=0$, m=1,2, the conditions for the stationary configuration reduces to

$$\begin{split} \hat{\mathfrak{D}}\phi_{n}^{(v)} &\equiv (\phi_{n+1}^{(v)} - \phi_{n}^{(v)}) - (\phi_{n}^{(v)} - \phi_{n-1}^{(v)}) = \\ &= (\phi_{n,1}^{(h)} - \phi_{n-1,1}^{(h)}) - (\phi_{n,2}^{(h)} - \phi_{n-1,2}^{(h)}), \end{split} \tag{13}$$

$$\phi_{n+1}^{(v)} - \phi_n^{(v)} = \phi_{n,1}^{(h)} - \phi_{n,2}^{(h)}. \tag{14}$$

One can easily observe that Eq. (13) can be obtained by subtracting Eq. (14) for n and n+1. At this point we notice that there are two possibilities to have stationary compact fluxon solutions:

(i) If one takes into account the fact that $\phi_{1,n}^{(h)} = -\phi_{2,n}^{(h)}$, which follows directly from Eqs. (7)-(11), we arrive to the single equation

$$\phi_{n,1}^{(h)} = \frac{1}{2} \left(\phi_{n+1}^{(v)} - \phi_n^{(v)} \right), n = \overline{1, N}. \tag{15}$$

The states that satisfy Eq. (15) will be referred to as anti-symmetric because they are anti-symmetric with respect to the "top"-"bottom" inversion.

(ii) There is another possibility. One can set either $\phi_{n,1}^{(h)}=0$, or $\phi_{n,2}^{(h)}=0$ for $n=\overline{1,N}$. Without loss of generality assume $\phi_{n,2}^{(h)}=0$, then

$$\phi_{n,1}^{(h)} = \phi_{n+1}^{(v)} - \phi_n^{(v)}, n = \overline{1, N}. \tag{16}$$

The conditions (15) or (16) can produce the infinite number of stationary states. In this work we will restrict ourselves to the elementary topological states (fluxons) and their most trivial combinations.

Elementary fluxons. These are the step-like solutions that connect two different ground states at the left and right sides of the ladder. The anti-symmetric fluxons can be written explicitly as

$$\phi_n^{(v)} = \begin{cases} \arcsin\gamma, & n \le n_0, \\ 2\pi Q + \arcsin\gamma, & n > n_0 \end{cases}, n = \overline{1, N+1}, (17)$$

$$\phi_{n,1}^{(h)} = -\phi_{n,2}^{(h)} = \pi Q \delta_{nn_0}, \quad n = \overline{1, N}. \tag{18}$$

The asymmetric compact states have the same distribution of the vertical phases but the horizontal phases must satisfy

$$\phi_{n,1}^{(h)} = 2\pi Q \delta_{nn_0}, \ \phi_{n,2}^{(h)} = 0, \ n = \overline{1, N},$$
 (19)

 $\phi_{n,1}^{(h)} = 0, \ \phi_{n,2}^{(h)} = -2\pi Q \delta_{nn_0}, \ n = \overline{1, N}$ (20)

These asymmetric states serve as a good demonstration of the importance of the full system of equations of motion that include both the top and bottom subsystems (dropped in Ref. [10]). Despite the top-bottom antisymmetry of the equations of the motion (7)-(11), there are dynamical solutions like discrete breathers [6, 11, 14] that break this symmetry. Since the values of the horizontal and vertical phases are connected, we can define a coding sequence that uses the vertical phase distribution in order to describe the total solution. For example, the 4π elementary fluxon will be denoted as $(\cdots 0, 4\pi, \cdots)$ and the 2π antifluxon will be denoted as $(\cdots 0, -2\pi, \cdots)$.

We reiterate that these compact states are exact solutions of the equations of motion (7)-(11). They are not possible for the standard parallel Josephson junction array that is governed by the DSG equation $\mathcal{N}(\phi_n) = \mathfrak{D}\phi_n + \gamma$. In DSG it is not possible to have a compact state, say $(\cdots 0, 2\pi, \cdots)$, because the phases decay asymptotically to the values 0 and 2π as $n \to \pm \infty$. The inductive energy $\propto \sum_n (\phi_{n+1} - \phi_n)^2$ can not reach its global minimum, however, in the JJL case the inductive energy is $\propto (\phi_{n+1}^{(v)} - \phi_n^{(v)} + \phi_{n,2}^{(h)} - \phi_{n,1}^{(h)})^2$. From here one can see that it is possible to nullify the energy by choosing the horizontal phases appropriately.

Combinations of the elementary fluxons. It is straightforward to conclude, that all possible superpositions of compact fluxons and antifluxons separated by an arbitrary number of sites will also be the stationary solutions of the equations of motion. The M-fluxon or a multi-fluxon state that consists of M fluxons with charges $Q_j > 0, \ j = \overline{1,M}$, centered at the points $1 < n_1 < n_2 < \cdots < n_M < N$ has the following dis-

tribution of the vertical phases:

$$\phi_n^{(v)} = \begin{cases} \arcsin \gamma, & n \le n_1, \\ 2\pi Q_1 + \arcsin \gamma, & n_1 < n \le n_2, \\ 2\pi (Q_1 + Q_2) + \arcsin \gamma, & n_2 < n \le n_3, \\ \dots \\ 2\pi \sum_{m=1}^M Q_j + \arcsin \gamma, & n > n_M, \end{cases}$$

$$n = \overline{1, N+1}.$$

And the distribution of the horizontal phases, for both the anti-symmetric and asymmetric fluxons, are given by the followin expression

Anti-sym.:
$$\phi_{n,1}^{(h)} = \pi \sum_{j=1}^{M} Q_j \delta_{n,n_j} = -\phi_{n,2}^{(h)},$$
 (22)

Asym.:
$$\phi_{n,1}^{(h)} = 2\pi \sum_{j=1}^{M} Q_j \delta_{n,n_j}, \phi_{n,2}^{(h)} = 0.$$
 (23)

It should be noted that the positions of the fluxons that constitute a combiden state should not coincide. Suppose we have $n_1 = n_2$, then we will obtain an elementary fluxon (17) with the total charge $Q_1 + Q_2$. Construction of the M-antifluxon state with topological charges Q_j $0, j = \overline{1, M}$ is straightforward.

It is possible to construct states with total zero topological charge. For example, the bound state of two oppositely charged fluxons with $\nu > 0$ vertical junctions between them is expressed as

$$\phi_n^{(v)} = \begin{cases} \arcsin \gamma, & n \le n_0, n > n_0 + \nu, \\ 2\pi Q + \arcsin \gamma, & n_0 < n \le n_0 + \nu, \end{cases}$$
(24)

$$n = \overline{1, N + 1},$$

$$n = \overline{1, N + 1},$$

$$\phi_{n,1}^{(h)} = \pi Q \delta_{n,n_0} = -\phi_{n_0,2}^{(h)},$$

$$\phi_{n_0+\nu,1}^{(h)} = -\pi Q \delta_{n,n_0+\nu} = -\phi_{n_0+\nu,2}^{(h)},$$

$$Asym.: \phi_{n,1}^{(h)} = 2\pi Q \delta_{n,n_0} = -\phi_{n_0+\nu,2}^{(h)}; \phi_{n,2}^{(h)} = 0,$$

$$n = \overline{1, N}$$

$$(25)$$

Asym.:
$$\phi_{n,1}^{(h)} = 2\pi Q \delta_{n,n_0} = -\phi_{n_0+\nu,2}^{(h)}; \quad \phi_{n,2}^{(h)} = 0, \quad (26)$$

$$n = \overline{1.N}.$$

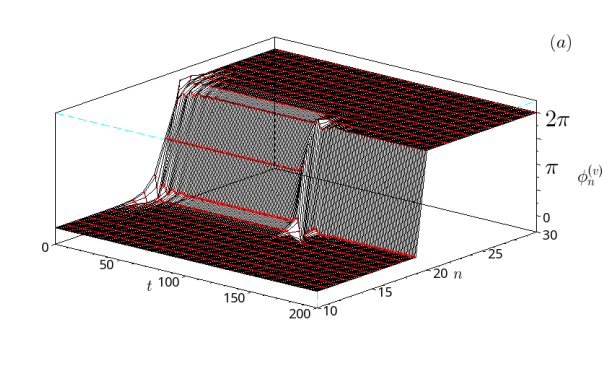
One can move further by creating various combinations of states (21)-(23) and (24)-(26).

The next logical step is to investigate the stability of these compact solutions. There are two ways of doing that. One way is to minimize numerically the ladder energy (12) and find the stable configurations. We have used another approach (also used in Ref. [10]) which was to solve numerically the equations of motion until the system settles on the stable stationary solution (attractor). The equations of motion (7)-(11) were solved numerically using the 4th order Runge-Kutta method with the initial condition that corresponds to the non-compact fluxon in the vertical subsystem and unperturbed horizontal subsystem:

$$\begin{split} \phi_n^{(v)} &= \arcsin \gamma + 4Q \arctan e^{\frac{n-n_0+\delta}{d}}, \ n = \overline{1,N+1}, \\ \phi_{n,m}^{(h)} &= 0, \ m=1,2, \ n = \overline{1,N}. \end{split} \tag{27}$$

Here d is initial fluxon width, n_0 is its initial position and $0 \le \delta \le 1/2$ is used to produce a junctioncentered ($\delta = 0$) or between-junction-centered or cellcentered ($\delta = 1/2$) stationary fluxon. The initial width is chosen according to the continuum sine-Gordon theory $d=1/\sqrt{\beta_L}$. In these simulations the dissipation parameter α controls only the speed of relaxation to the equilibrium, and, therefore, can be chosen arbitrarily. We take it $\alpha = 0.25$ unless stated otherwise.

The results of such simulations are presented in Fig. 2. What is observed can be called the *compactification*



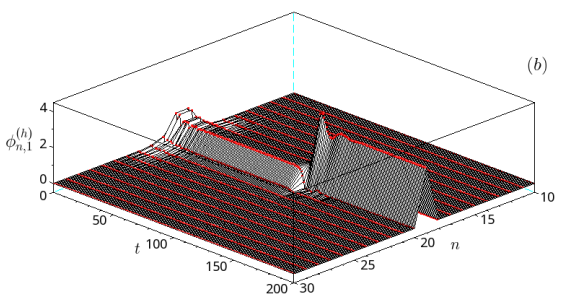


FIG. 2: Fluxon profile compactification for the vertical (a) and bottom horizontal (b) junctions as a function of time for the discreteness $\beta_L = 1.5$, bias $\gamma = 0$ and anisotropy $\eta = 0.5$. The ladder size is N = 40.

process when the initially non-compact profile gradually becomes more localized and, finally, ends up as an antisymmetric compact fluxon that satisfies Eqs. (17)-(18). The time evolution of the top horizontal junctions was not plotted for the sake of brevity.

A detailed analysis of the vertical phase behavior during the compactification process is given in Fig. 3. The time evolution of the $(n_0 - 1)$ th junction on the $(\phi_{n_0-1}^{(v)},\dot{\phi}_{n_0-1}^{(v)})$ phase plane shows that it indeed converges to the zero value.

It is possible to observe the fluxon compactification to the asymmetric state given by Eqs. (17), (19)-(20). In this case the initial conditions were modified. The initial vertical phase distribution was chosen as in Eq. (27), the

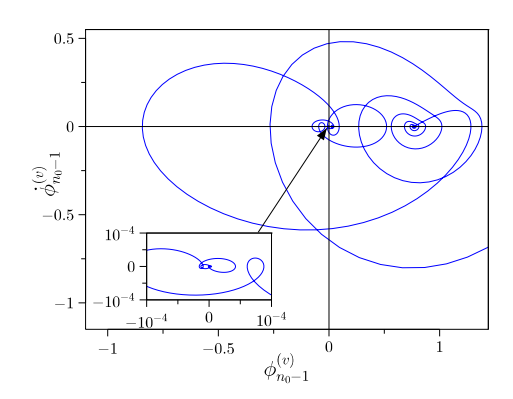


FIG. 3: Time evolution of the $(n_0 - 1)$ vertical junction for the case described in Fig. 2.

bottom horizontal was phases were chosen as

$$\phi_{n,1}^{(h)} = 0, \ \phi_{n,2}^{(h)} = -\frac{1}{\cosh\left(\frac{n-n_0+\delta}{d}\right)}, \ n = \overline{1, N}.$$
 (28)

For the simulations we have taken $\delta=0.5$. The results are shown in Fig. 4. One can observe that the compatification process is happening rather fast and the final configuration becomes compact and asymmetric (with respect to the top-bottom inversion) as prescribed by Eqs. (17), (19)-(20). It is seen very clearly that the central bottom horizontal junction tends to the value 2π while the rest approach 0. The top horizontal subsystem junctions tends to the unexcited ground state $\phi_{n,2}^{(h)}=0$. We have performed similar simulations for the differ-

We have performed similar simulations for the different values of η and β_L as well as for the higher topological charges. We have observed that the compactification process happens for smaller values of η while for larger anisotropies the system ends on the non-compact state. We find it to be useful to investigate the dependence of the compactification process on the anisotropy constant η together with calculating the stationary fluxon energy.

B. Energies of the compact and non-compact fluxons

The energies of the compact stationary fluxons can be calculated analytically by substituting the exact solutions (17), (18) and (19-20) into the JJL energy (12). The energies of the elementary anti-symmetric (E_{ANS}) and asymmetric (E_{A-S}) fluxons for a given topological charge $Q \in \mathbb{Z}$ can be written as

$$E_{ANS}[Q] = 2[1 - (-1)^{Q}]\eta + D_{Q}(\gamma, n_{0}, N), \qquad (29)$$

$$E_{A-S}[Q] = D_Q(\gamma, n_0, N),$$
 (30)

$$D_Q(\gamma, n_0, N) = N(1 - \sqrt{1 - \gamma^2} - \gamma \arcsin \gamma) - 2\pi Q(N - n_0)\gamma.$$
(31)

Here the term $D_Q(\gamma, n_0, N)$ appears because the dc bias makes the potential minima for the $\phi = \arcsin \gamma$

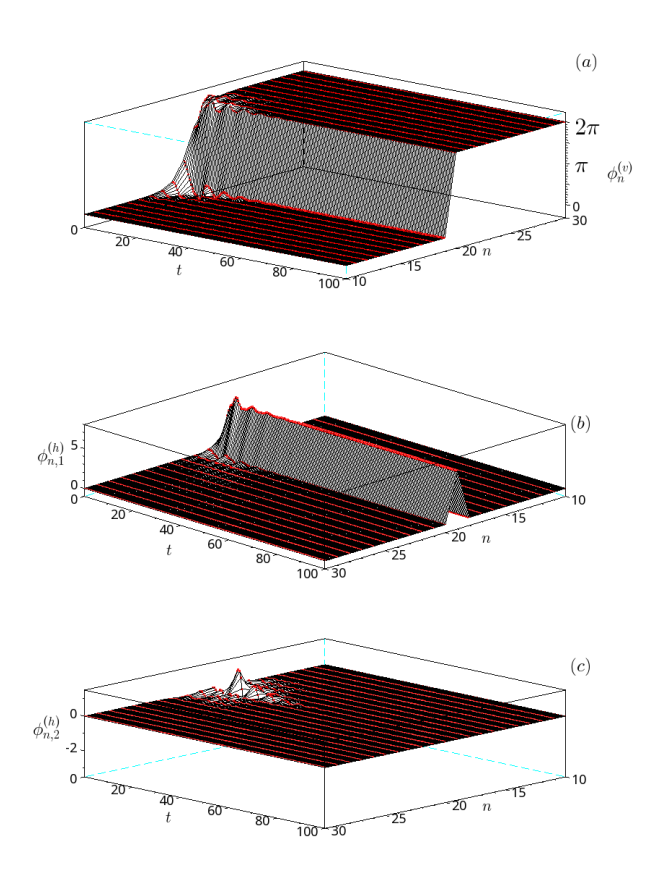
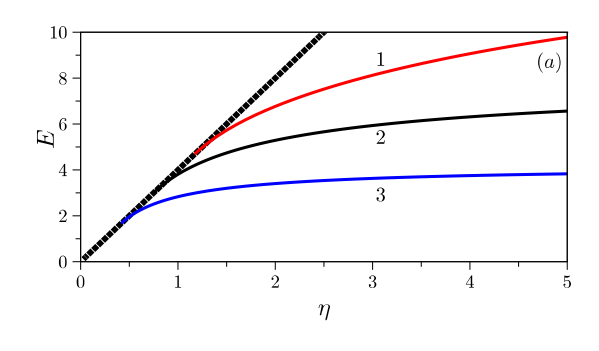


FIG. 4: Fluxon profile compactification for the vertical (a), horizontal bottom (b) and top (c) junctions as a function of time for the same parameters as in Fig. 2.

and $\phi = 2\pi Q + \arcsin \gamma$ non-equivalent. Naturally, $D_Q(\gamma = 0, n_0, N) = 0$. Let us assume for a while that the $\gamma = 0$. The energy for the anti-symmetric fluxons with even topological charges is exactly zero while for the odd charges it equals 4η . The difference comes from the Josephson energy of the horizontal phases at the $n = n_0$ site where $\phi_{n_0,1}^{(h)} = -\phi_{n_0,2}^{(h)} = Q\pi$. Each of these junctions contributes the value of 2η to the total energy. When Q is even these sites correspond to the energy minima, and, consequently, the total fluxon energy is zero. The energy of the asymmetric states is always zero (up to a constant D_Q). The energy of the multi-fluxon state defined by Eqs. (21)-(22) is a sum of the energies of the constituting elementary fluxons. Here lies the difference between the elementary fluxon (17)-(18) with some even topological charge and the multi-fluxon state (21)-(22) with two fluxons with odd topological charges Q_1 and $Q_2, Q_1 + Q_2 = Q$. Provided $\gamma = 0$, the energy of the former state equals 0 while the energy of the latter state is $4\eta(Q_1+Q_2)$. In the analogous case of asymmetric elementary and multi-fluxon states the energy would be zero (if $\gamma = 0$) in both cases. The difference would be hidden in the constant D_Q which should be redefined appropriately for the multi-fluxon case.

In order to compare the energies of the non-compact

and compact fluxon states the total energy (12) was computed numerically as a function of the anisotropy η and for the different values of the discreteness constant β_L . The results for the unbiased $(\gamma = 0)$ Q = 1 fluxon are shown in Fig. 5(a). The non-compact fluxon state is computed by integrating numerically Eqs. (7)-(11) with the initial conditions (27). We have started from the limit of large η . In this case the system converges to the non-compact stationary fluxon. The additional initial distortion (28) of the horizontal subsystem is not important, the system settles on the same stationary state. As the anisotropy is decreased the fluxon energy decreases as well. At some critical anisotropy, η_c , the fluxon energy equals the respective energy of the anti-symmetric compact state, 4η . At this point and further on, for $\eta < \eta_c$, the system settles on the anti-symmetric compact fluxon state. The point $\eta = 0$ should be excluded, because



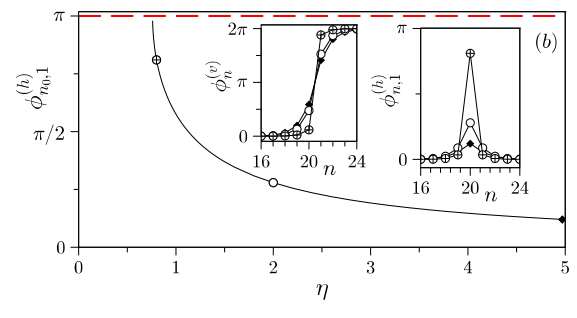


FIG. 5: (a) Energy of the non-compact stationary fluxons as a function of the anisotropy η for $\beta_L=0.25$ (line 1, red), $\beta_L=1$ (line 2, black) and $\beta_L=3$ (line 3, blue). The straight line (\blacklozenge) corresponds to the energy of the compact fluxon, $E=4\eta$. (b) Maximal value of the horizontal bottom phase, $\phi_{n_0,1}^{(h)}$ as a function of anisotropy for $\beta_L=1$. The dashed red line corresponds to the value $\phi_{n_0,1}^{(h)}=\pi$. The insets demonstrate the vertical $\phi_n^{(v)}$ and bottom horizontal $\phi_{n,1}^{(h)}$ distributions for $\eta=5$ (\spadesuit), $\eta=2$ (\circ) and $\eta=0.8$ (\oplus). The markers on the curve correspond to the above metioned values of η .

we have division by zero in Eqs. (8). However, in this case the horizontal system is completely decoupled from the vertical subsystem which is governed by the standard DSG equation.

The non-compact fluxon energy is larger for the smaller values of β_L because the inductive energy is proportional to $1/\beta_L$. Also, the critical anisotropy, η_c , increases when

 β_L is decreased. It is instructive to see how the noncompact fluxon shape changes with the decrease of $\eta.$ In Fig. 5(b) we show how the maximum of the bottom horizontal phase distribution changes with $\eta.$ The insets depict the fluxon profiles in the vertical and bottom horizontal subsystems. We observe that the fluxon becomes more localized as η is decreased. The top horizontal phase is not plotted because $\phi_{n_0,2}^{(h)} = -\phi_{n_0,1}^{(h)}.$ The maximal value $\phi_{n_0,1}^{(h)}$ also increases when η is decreased until it reaches the value of π at $\eta = \eta_c.$ Below $\eta < \eta_c$ only compact fluxons exist.

It is of interest to see what happens if one simulates the equations of motion with compact initial conditions. We have found that states with zero energy, i.e., the antisymmetric with even topological charges and asymmetric ones, persist. The compact anti-symmetric odd-charged fluxon initial conditions evolve into the non-compact fluxon for $\eta > \eta_c$ and remain compact for $\eta < \eta_c$. However, these states are not fully stable either. We have found that they are unstable against only one type of perturbation. The deviation of the central horizontal phase, either $\phi_{n_0,1}^{(h)} = \pi + \epsilon$ or $\phi_{n_0,2}^{(h)} = -\pi + \epsilon$, facilitates the transition to the asymmetric state (19) or (20). Any other perturbation, including the anti-symmetric one of the type $\phi_{n_0,1}^{(h)} = \pi + \epsilon$, $\phi_{n_0,2}^{(h)} = -\pi - \epsilon$, leaves the anti-symmetric odd-charged fluxon intact. The possible explanation must be connected with flat band in the linear wave spectrum [7] and the consequent absence of dispersion.

If the dc bias is applied, the general situation remains the same. In Fig. 6 we show again the energy of the non-compact fluxon as a function of η but for the biased JJL with $\gamma = 0.1$. The only difference with the unbiased

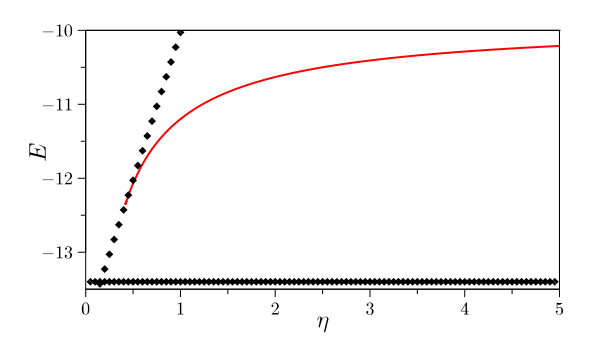


FIG. 6: Energy of the non-compact stationary fluxons as a function of the anisotropy η for $\beta_L = 1$ and $\gamma = 0.1$. The straight lines (\spadesuit) corresponds to the energy of the compact anti-symmetric and asymmetric fluxons.

case [Fig. 5(a)] is in the absolute energy values since the constant D_Q which is given by Eq. (31) is no longer zero.

Now we turn our attention towards the multi-fluxon stationary states. We repeat the same numerical experiment by starting with the non-compact bi-fluxon (Q=2) state and reducing the anisotropy. The multi-fluxon

stationary states demonstrate more complex behavior. Firstly, the multi-fluxon family is much diverse because there is an additional possibility to have different spatial separation between the individual fluxons. Also, both the stable junction-centered (with the fluxon center on a vertical junction) and cell-centered (the fluxon center lies in the middle of the junction cell, or, alternatively, in the center of the junction cell) can exist. We have found only stable cell-centered Q = 1 fluxons [see the left inset in Fig. 5(b)]. In Fig. 7 the dependence of the non-compact fluxon energy on the anisotropy is shown. In order to obtain a multi-fluxon with a certain symmetry we have used different parameter δ in the initial condition (27). We have observed in our simulations that for $\delta = 0, 0.1, 0.2$ the system is attracted to the junction-centered state and for $\delta = 0.4, 0.5$ is is attracted to the cell-centered state. The cell-centered bi-fluxon has smaller energy and transforms into the compact anti-symmetric $(...0, 2\pi, 2\pi, 4\pi, ...)$ bi-fluxon at $\eta \approx 0.5$ when its energy coincides with the 8η line. The junction-centered non-compact bi-fluxon (red line) has larger energy and jumps into the compact elementary asymmetric Q = 2 fluxon (17)-(19) with zero energy. The critical anisotropy value η_c that separates the compact and non-compact states is larger for the bi-fluxon with the junction-centered symmetry.

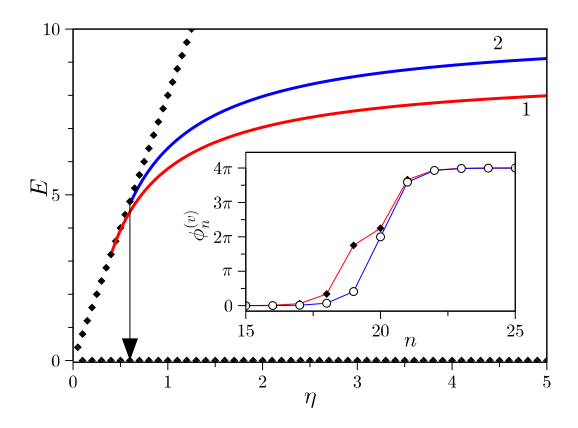


FIG. 7: Energy of the non-compact cell-centered (line 1, red) and junction-centered (line 2, blue) stationary fluxons with topological charge Q=2 as a function of the anisotropy η for $\beta_L=3$ and $\gamma=0$. The straight lines (\blacklozenge) corresponds to the energy of the compact anti-symmetric ($E=8\eta$) and asymmetric (E=0) bi-fluxons. The inset shows the cell-centered (\blacklozenge) and junction-centered \circ fluxon profiles at $\eta=2$.

We have also performed simulations for the smaller values of β_L . Smaller β_L causes the non-compact fluxons to be more spread out. As a result, the critical point $\eta = \eta_c$ the compactification process brings a composite bi-fluxon of the type (17)-(18) with larger separation between the constituent fluxons. Compactification of the Q=3 multi-fluxons was also observed.

The application of magnetic field $(f \neq 0)$ destroys the

compact solutions since it becomes impossible to satisfy the stationary part of Eqs. (7)-(11) in such a way that all the phases are the same. However, if the magnetic field is small, the non-compact states are strongly localized as the anisotropy approaches zero. The energy-anisotropy dependencies for the elementary fluxons is shown in Fig. 8. The functions $E(\eta)$ are smooth, but their behavior at small η is almost linear. The profiles of the vertical phase

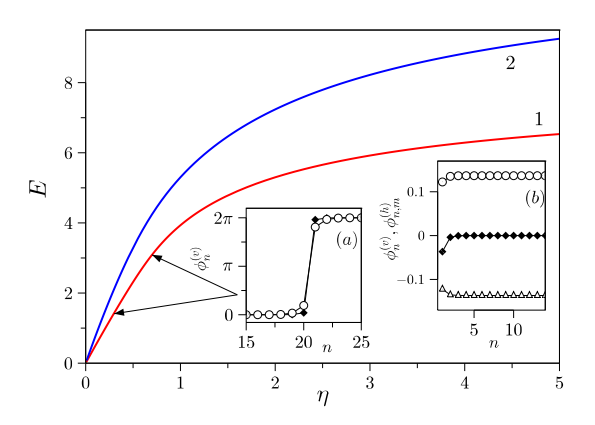


FIG. 8: Stationary fluxon energy a function of η for $\beta_L=1$, $\gamma=0$ and magnetic field f=0.05 (line 1, red) and f=0.1 (line 2, blue). The inset (a) shows the central part of the vertical phase distribution for $\eta=0.3$ (\blacklozenge) and $\eta=0.7$ (\circ). The inset (b) depicts the tail behavior of the three components, $\phi_n^{(v)}$ (\blacklozenge), $\phi_{n,1}^{(h)}$ (\triangle) and $\phi_{n,2}^{(h)}$ (\circ) for $\eta=0.3$, f=0.05.

distribution [see the inset (a) in Fig.8] show that although the fluxons are no longer exactly compact, they are very strongly localized. The fluxon tails show small distortion cause by the breaking of the translation symmetry by the field.

IV. COMPACT FLUXON INTERACTION WITH THE PLANE WAVES

Finally we investigate the interaction of stationary compact fluxons with the small-amplitude waves of the ladder (Josephson plasmons). In order to launch a plasmon we replace the dc bias γ in the equation for the n=1vertical junction by the mixed dc-ac bias $\gamma + \gamma_{ac} \sin \omega t$. The stationary compact anti-symmetric fluxon with Q =1 is placed in the middle of the ladder at $n_0 = N/2$. The results of simulations of equations of motion (7)-(11) are shown in Fig. 9. The dissipation constant was chosen rather small ($\alpha = 0.01$) in order to minimize the spatial and temporal decay of the plasmon amplitude. The total integration time was $t = 2 \times 10^4$. So, the threecomponent plasmon wave is scattered on the stationary compact fluxon. The plasmon dispersion law has three branches [7] has three branches, one is strongly dispersive, one is weakly dispersive and one is flat with $\Omega = 1$. The weakly dispersive branch is also flat if $\gamma = 0$. For the JJL parameters $\eta=0.5$, $\beta_L=1$ the frequencies of the strongly dispersive branch lie in the interval $\sqrt{5}<\Omega<3$. The highest plasmon density of states is achieved on the borders of the plasmon band [15]. Therefore, we have chosen two values of the driving frequency, one close to the bottom of the band, $\omega=2.3$, and one close to the top of the band, $\omega=2.98$. As a result of interaction the com-

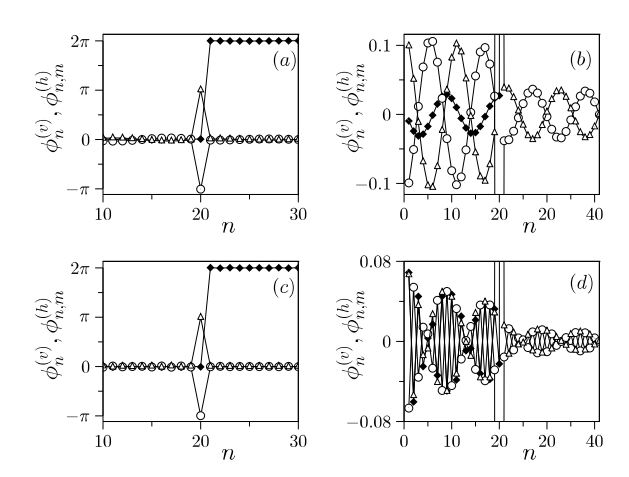


FIG. 9: Final fluxon profiles $\phi_n^{(v)}$ (\spadesuit), $\phi_{n,1}^{(h)}$ (\triangle) and $\phi_{n,2}^{(h)}$ (\circ) in the ladder with N=40, $\eta=0.5$, $\beta_L=1$ and $\alpha=0.01$. The ac bias parameters are $\gamma=0$, $\gamma_{ac}=0.3$, $\omega=2.3$ [(a) and (b)] and $\omega=2.98$ [(c) and (d)]. The panels (b) and (d) show the details of the plasmon distribution for the panels (a) and (c), respectively.

pact fluxon survives and preserves its strongly localized shape [see Fig. 9(a) and 9(c)]. The plasmon transmission is not perfect as the outgoing plasmon amplitude is approximately halved. Part of the plasmon energy is absorbed by the fluxon. Earlier in this paper we have stated that the Q=1 anti-symmetric compact fluxon is not stable. However, the plasmon is polarized in such a way that the top-bottom antisymmetry is preserved. This is clearly seen in Figs. 9(b) and 9(d). Thus, the fluxon receives the anti-symmetric perturbation, and, as it was stated before, it is stable against such a perturbation. More detailed research on the plansmon-fluxon interaction is underway and will be reported elsewhere.

V. CONCLUSIONS

In this work a new type of topological states that exist in Josephson junction ladders (JJLs) has been discovered. These states are stationary compact fluxons that connect different ground states of the ladder and are exact solutions of the respective equations of motion. They are compact in the strict sense: the respective Josephson phases attain the values that are exact equilibrium values of the individual junctions throughout the whole ladder. In other words, the phase distribution in the subsystem of the vertical junctions is an exact step-like function of the junction number. The energies of the compact states can be written explicitly. They are stable for the wide domain of the system parameters. They coexist with the non-compact solutions if the anisotropy constant η is large enough and are the only stable stationary states if $0 < \eta < \eta_c(\beta_L)$. This can be interpreted as an integrable sector of the JJL, since the only existing topological states are the compact ones and their energy is known.

Compact stationary fluxons exist for the dc-biased ladder, however, their compactness is destroyed by any (even very small) external magnetic field. The existence of compact states is connected to the fact that the linear dispersion law of the JJL has a flat band. Hence, apart from the states that decay exponentially $[\phi_n(n \to -\infty) \sim e^{-\lambda n}]$ and are non-compact, there can be states whose decay factor λ is exactly zero. Compact states are not possible in the parallel Josephson junction arrays. The parallel array is governed by the DSG equation and supports only exponentially decaying noncompact fluxons.

Acknowledgements

We would like to thank the Armed Forces of Ukraine for providing security to perform this work. I.O.S. and Y.Z. acknowledge support from the National Research Foundation of Ukraine, grant (2023.03/0097) "Electronic and transport properties of Dirac materials and Josephson junctions".

^[1] M. Kardar, Phys. Rev. B **30**, 6368 (1984).

^[2] C. Denniston and C. Tang, Phys. Rev. Lett. **75**, 3930 (1995)

^[3] L. M. Floria, J. L. Marin, S. Aubry, P. J. Martinez, F. Falo, and J. J. Mazo, Physica D 113, 387 (1998).

^[4] S. Watanabe, H. S. J. van der Zant, S. H. Strogatz, and T. P. Orlando, Physica D 97, 429 (1996).

^[5] E. Trías, J. J. Mazo, and T. P. Orlando, Phys. Rev. Lett. 84, 741 (2000).

^[6] P. Binder, D. Abraimov, A. V. Ustinov, S. Flach, and Y. Zolotaryuk, Phys. Rev. Lett. 84, 745 (2000).

^[7] A. E. Miroshnichenko, S. Flach, M. V. Fistul,

Y. Zolotaryuk, and J. B. Page, Phys. Rev. E **64**, 066601 (2001)

^[8] D. Bukatova and Y. Zolotaryuk, Journal of Physics: Condensed Matter 34, 175402 (2022).

^[9] J. J. Mazo, F. Falo, and L. M. Floría, Phys. Rev. B 52, 10433 (1995).

^[10] G. Grimaldi, G. Filatrella, S. Pace, and U. Gambardella, Phys. Lett. A 223, 463 (1996).

^[11] E. Trías, J. J. Mazo, and T. P. Orlando, Phys. Rev. B 65, 054517 (2002).

^[12] P. G. Kevrekidis, V. V. Konotop, A. R. Bishop, and S. Takeno, Journal of Physics A: Mathematical and Gen-

- eral $\bf 35$, L641 (2002). [13] F. K. Abdullaev, P. G. Kevrekidis, and M. Salerno, Phys. Rev. Lett. **105**, 113901 (2010).
- [14] P. Binder, D. Abraimov, and A. V. Ustinov, Phys. Rev.
- E **62**, 2858 (2000). [15] D. Bukatova, I. O. Starodub, and Y. Zolotaryuk, Phys. Lett. A **562**, 130983 (2025).